JGR Earth Surface

RESEARCH ARTICLE
10.1029/2018JF004707

Contrasting Hydrological Controls on Bed Properties During the Acceleration of Pine Island Glacier, West Antarctica

M. Bougamont[1], P. Christoffersen[1], I. Nias[2,3,4], D. G. Vaughan[5], A. M. Smith[5], and A. Brisbourne[5]

[1]Scott Polar Research Institute, University of Cambridge, Cambridge, UK, [2]Bristol Glaciology Centre, University of Bristol, Bristol, UK, [3]Now at Earth System Science Interdisciplinary Center, University of Maryland, College Park, MD, USA, [4]Cryospheric Sciences Laboratory, Goddard Space Flight Center, NASA, Greenbelt, MD, USA, [5]British Antarctic Survey, Natural Environment Research Council, Cambridge, UK

Abstract In the Amundsen sector of West Antarctica, the flow of glaciers accelerates when intrusion of warm ocean water onto the continental shelf induces strong melting beneath ice shelves and thinning near the glaciers' grounding line. Predicting the future of these glaciers is, however, hindered by a poor understanding of the dynamical processes that may exacerbate, or on the contrary modulate, the inland ice sheet response. This study seeks to investigate processes occurring at the base of Pine Island Glacier through numerical inversions of surface velocities observed in 1996 and 2014, a period of time during which the glacier accelerated significantly. The outputs show that substantial changes took place in the basal environment, which we interpret with models of undrained subglacial till and hydrological routing. The annual basal melt production increased by 25% on average. Basal drag weakened by 15% over nearly two thirds of the region of accelerated flow, largely due to the direct assimilation of locally produced basal meltwater into the underlying subglacial sediment. In contrast, regions of increased drag are found to follow several of the glacier's shear margins and furthermore to coincide with inferred hydrological pathways. We interpret this basal strengthening as signature of an efficient hydrological system, where low-pressure water channels have reduced the surrounding basal water pressure. These are the first identified stabilization mechanisms to have developed alongside Pine Island ice flow acceleration. Indeed, these processes could become more significant with increased meltwater availability and may limit the glacier's response to perturbation near its grounding line.

Key Points:
- Numerical inversions interpreted with undrained till and water routing models are used to infer basal changes and hydrological conditions
- Weaker beds in central troughs are offset by stronger beds along shear margins, which coincide with major hydrological pathways
- The future flow of PIG may depend on the coevolution of basal properties and shear margins in addition to its interaction with the ocean

Supporting Information:
- Supporting Information S1

Correspondence to:
M. Bougamont,
mb627@cam.ac.uk

Citation:
Bougamont, M., Christoffersen, P., Nias, I., Vaughan, D. G., Smith, A. M., & Brisbourne, A. (2019). Contrasting hydrological controls on bed properties during the acceleration of Pine Island Glacier, West Antarctica. *Journal of Geophysical Research: Earth Surface*, *124*, 80–96. https://doi.org/10.1029/2018JF004707

Received 10 APR 2018
Accepted 18 DEC 2018
Accepted article online 21 DEC 2018
Published online 17 JAN 2019

1. Introduction

Pine Island Glacier (PIG) is a fast-flowing glacier, which drains the West Antarctic Ice Sheet. Flowing into the Amundsen Sea, the glacier has significantly accelerated since the 1970s (Crabtree & Doake, 1982; Williams et al., 1982). The net ice loss associated with this acceleration currently contributes to ~0.12 mm/yr of global sea level rise and is responsible for 20% of the net annual mass loss from West Antarctica (Medley et al., 2014; Rignot, Velicogna, et al., 2011; Wingham et al., 2009).

The causes of the dynamical changes observed near the grounding line of PIG have been widely attributed to oceanographic conditions (Dutrieux et al., 2014; Jacobs et al., 2011; Jenkins et al., 2010; Payne et al., 2004; Steig et al., 2012), with inflow of relatively warm circumpolar deep water increasing basal melting of its ice shelf (Jacobs et al., 1996). The thinning of the ice shelf drives retreat of the grounding line and reduces buttressing on the glacier, both of which lead to grounded ice flow acceleration (Cornford et al., 2015; De Rydt & Gudmundsson, 2016; Favier et al., 2014; Goldberg et al., 2012; Joughin et al., 2010; Schoof, 2007).

The effect of ice shelf thinning alone is, however, not sufficient to explain the observed acceleration of the inland ice flow, for which the additional impact of dynamical thinning must also be accounted for (Scott et al., 2009). Recently, the rate of flow acceleration near the grounding line has decreased (Joughin et al., 2010; Shen et al., 2018), yet PIG remains out of balance and the inland flow continues to experience acceleration and thinning, albeit at rates varying considerably over the extent of the glacier (Konrad et al., 2017). It has been suggested that this heterogeneous ice flow evolution may be due to

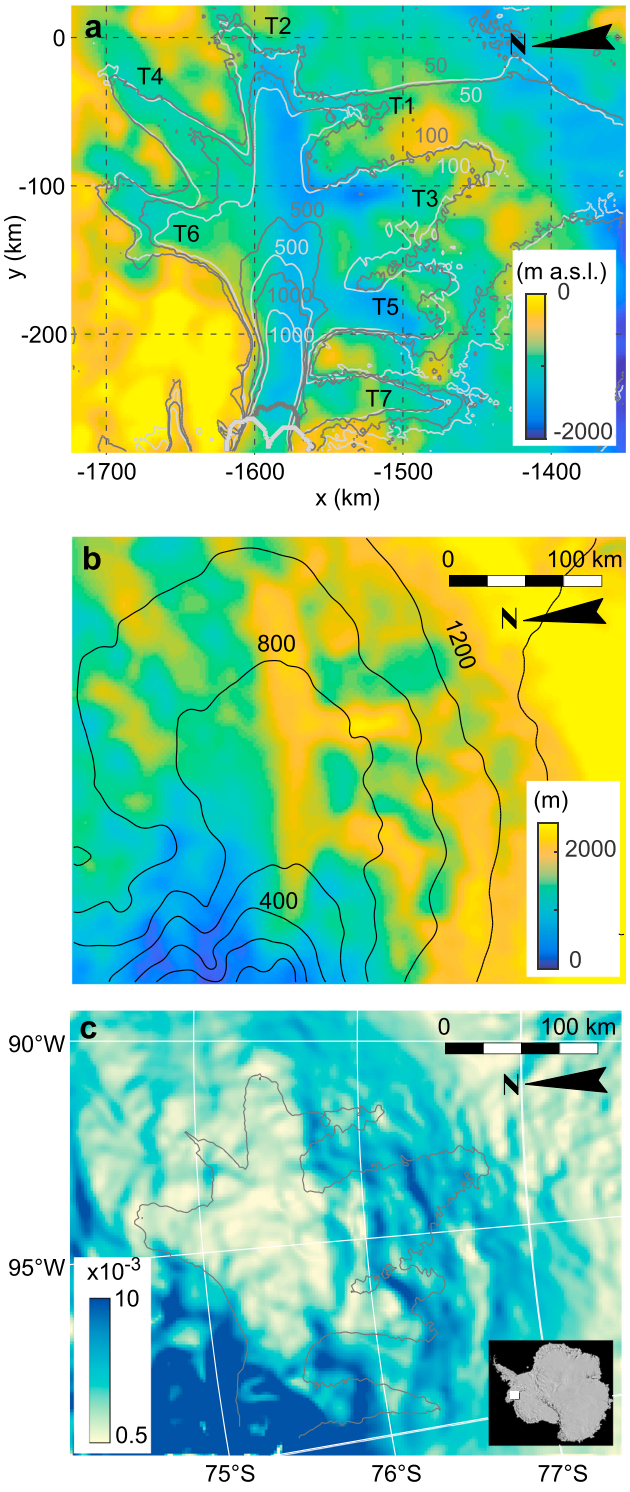

Figure 1. (a) Bed topography (m above sea level) of Pine Island Glacier overlain with observed surface velocity contours (m/yr) and grounding line position, in 1996 (light gray lines) and 2014 (dark gray lines). The seven tributaries are labeled T1–T7. The domain coordinates (*x* and *y*) are given in the WGS84 Antarctic Polar Stereographic system. (b) Ice thickness (m) overlain with surface elevation contours (m, black lines), (c) Surface slopes (ND), overlain with the 100-m/yr velocity contour from 2014 (dark gray line). The inset locates the domain within Antarctica.

changes in basal conditions (Konrad et al., 2017), but little is known about the processes that control the evolving physical state of the subglacial environment of PIG.

The main trunk of PIG is fed by seven tributaries (T1–T7, Figure 1) underlain by contrasting topographic (Bingham et al., 2017; Vaughan et al., 2006), frictional (Gillet-Chaulet et al., 2016; Joughin et al., 2009), and geological properties (Brisbourne et al., 2017; Smith et al., 2013). The surface slopes of its northern tributaries (T4 and T6) are low, and the basal topography is relatively smooth (Figure 1). Over the main trunk, surface slopes are also low and ice flows over a deep trough where there is little basal resistance against ice flow (T2). In contrast, over the southern tributaries (T1-T3-T5-T7), the surface slopes are high, and the basal topography is much rougher (Figure 1).

Seismic data analysis (Brisbourne et al., 2017; Smith et al., 2013) and the inference of low basal drag from numerical inversion (Joughin et al., 2009) point to the widespread presence of glacially produced till, which is known to be the primary enabler of ice stream flow elsewhere in West Antarctica (Alley et al., 1986; Anandakrishnan, 2003; Bougamont et al., 2015; Christoffersen & Tulaczyk, 2003; Engelhardt & Kamb, 1998; Kamb, 2001; Retzlaff & Bentley, 1993; Tulaczyk et al., 1998, 2000b). For example, the layer of till beneath the Siple Coast ice streams is known to deform plastically (Kamb, 1991; Tulaczyk et al., 2000a), with the implication that small changes in pore water pressure within it can significantly alter its shear strength, and hence the speed of the overlying ice.

Interpretation of seismic reflection profiles collected beneath PIG (Brisbourne et al., 2017) suggests that till layers are composed of reworked marine sediments that may have been extensively deposited on the sea floor during the warm Pliocene period when the West Antarctic Ice Sheet had retreated significantly (DeConto & Pollard, 2016; Gasson et al., 2016; Pollard & DeConto, 2009). Although more direct observations of the characteristics of basal till come from Siple Coast ice streams (Tulaczyk et al., 1998, 2000a), we assume that till beneath PIG has broadly similar characteristics. This inference is supported by modeling studies showing good correspondence between modeled and observed ice flow when the basal conditions of PIG are assumed to be Coulomb-plastic (Gillet-Chaulet et al., 2016; Joughin et al., 2010). While previous work has shown that the physical properties of Coulomb-plastic tills evolve continuously and significantly beneath ice streams at the Siple Coast (Beem et al., 2014; Bougamont et al., 2015; Christoffersen et al., 2014; Elsworth & Suckale, 2016; Tulaczyk et al., 2000b; van der Wel et al., 2013), this evolution has been largely overlooked in studies of ice streams located in other regions of West Antarctica (Cornford et al., 2015; Favier et al., 2014; Gillet-Chaulet et al., 2016; Gladstone et al., 2012; Jamieson et al., 2012; Joughin et al., 2010; Parizek et al., 2013; Seroussi et al., 2014).

In order to assess the in/stability of PIG and quantify its contribution to sea-level rise over the coming decades, it is essential to understand how the basal processes control the inland ice flow. Hence, we seek to understand how, and why, basal properties have evolved during its recent observed speed-up. We take advantage of nearly two decades of observations of surface velocities to perform numerical inversions

and calculate variations in basal conditions over an 18-year period, seeking to identify and quantify changes in basal stress, melt rates, and hydrological pathways. We focus on the upper section of PIG's main trunk and its tributaries where glacier acceleration has been sustained. We show that over this period, increased production of meltwater due to faster glacier motion has caused two opposing responses in the basal environment. Whereas the bed of PIG has become physically weaker in central regions, the bed beneath shear margins and major hydrological pathways has become significantly stronger.

2. Methods

We study changes in the basal conditions of PIG over an 18-year period by inverting surface velocities observed in (a) 1996 and (b) 2014 using an ice sheet model (see section 2.1 for details). With an inferred Coulomb plastic till rheology, we equate the difference between the two basal traction fields to changes in till shear strength stemming from water that has either flowed into or out of a uniformly distributed basal till layer during the intervening 18-year period (section 2.2). To examine the nature of the hydrological conditions beneath PIG, we first quantify sources and sinks of water in the basal environment (section 2.3). The major hydrological pathways of the net available subglacial water are then investigated with a commonly used steady-state routing algorithm (section 2.3). This analysis is a quantitative interpretation of two steady-state solutions from numerical inversions, similar to the approach described in Christoffersen et al. (2014). As such, there is no dynamic feedback between the ice flow model, the subglacial till model, and the hydrological routing model.

2.1. Numerical Ice Flow Model and Inversion Method

We investigated the ice flow of PIG catchment by performing numerical inversions of basal traction using the surface velocities observed in 1996 (ERS1-2 from Joughin et al., 2009) and in 2014 (Sentinel data from Nagler et al., 2015), with grounding line positions mapped, respectively, using DInSAR and MOA data (Rignot, Mouginot, et al., 2011).

The inversions were performed on a fixed grid at 2-km resolution with the higher-order three-dimensional numerical ice flow model CISM 2.0, which solves the conservation of momentum, mass, and thermal energy, using finite difference methods (Dukowicz et al., 2010; Pattyn, 2003; Price et al., 2015). We apply Dirichlet conditions around the domain (e.g., shown in Figure 2a), with velocities imposed by the two velocity maps used for the inversions.

Modeled surface velocities were iterated toward observed values, first by prescribing a no-slip basal boundary condition, which allows internal ice deformation to evolve to equilibrium. We then subtracted this value from the target surface velocity iterating toward a pattern of basal traction and sliding rates, needed to fully converge ice temperature, effective ice viscosity, and ice velocity fields toward observed values. The full details of this method are described by Price et al. (2011), and its previous applications include other regions in Antarctica (Bougamont et al., 2015; Christoffersen et al., 2014) and Greenland (Bougamont et al., 2014; Price et al., 2011, 2017).

To constrain the inversions, we used a fixed glacier geometry consisting of the surface elevation provided in BEDMAP2 (Fretwell et al., 2013) and a bed elevation model derived from a mass conservation approach (Nias et al., 2018). The significant surface lowering observed after 2004 (Flament & Remy, 2012; Konrad et al., 2017; Wingham et al., 2009) is accounted for in the 2014 inversion, by estimating the difference between IceSat (2004–2006) and Cryosat-2 (2011–2013) observations (supporting information Figure S1). The distributed air temperature is given by Comiso (2000), the snow accumulation is from van de Berg et al. (2006), and the geothermal heat flux is from Shapiro and Ritzwoller (2004).

The final inversion consisted of distributions of basal melt rates ($\dot{m}$, m/yr) and traction (τ_b, Pa) calculated for 1996 and 2014, as well as the three-dimensional distribution of the converged ice flow velocity and englacial temperature, assuming basal temperature to be at the pressure melting point. The spatially distributed basal melt rates were calculated taking into account frictional heat, geothermal heat flux, conductive heat loss, and latent heat of fusion:

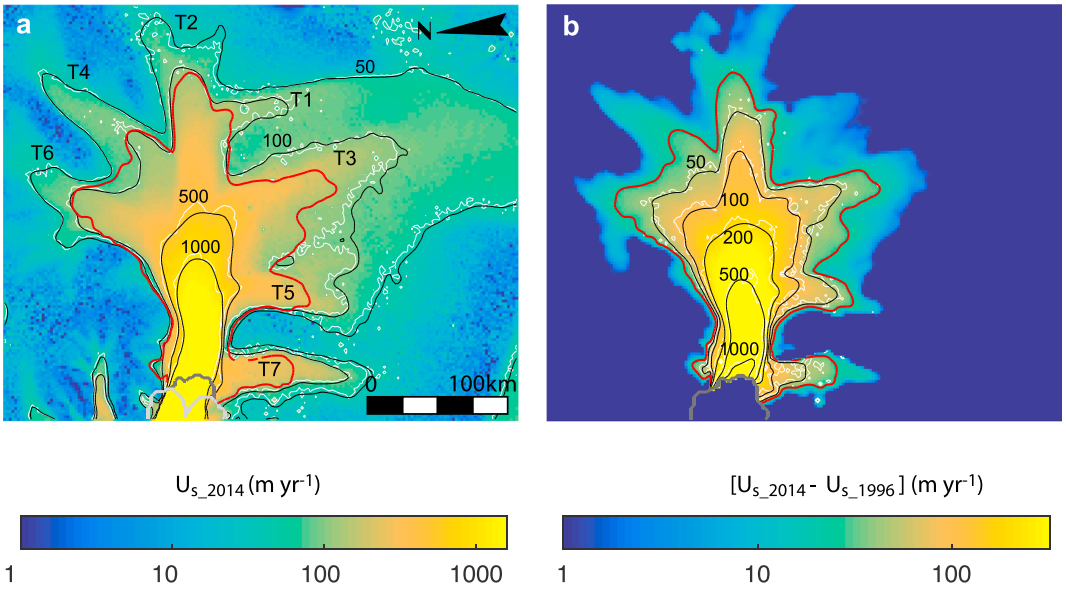

Figure 2. (a) Map of observed surface velocity in 2014 (m/yr), showing the position of the 1996 (light gray line) and 2014 (dark gray line) grounding lines. The map is overlain with contours of observed (white lines) and modeled (black lines) surface velocity. The area where speed-up exceeds 25 m/yr between 1996 and 2014 is outlined in red. The seven tributaries are labeled T1–T7. (b) Map of modeled surface velocity speed-up between 1996 and 2014, overlain with contours of observed (white) and modeled (black) velocity speed-up (as labeled). Red line is as in (a).

$$\dot{m} = \frac{U_b \tau_b + G - K_i \theta_b}{\rho_i L}, \tag{1}$$

where U_b is the basal ice velocity (m/yr), G is the geothermal heat flux (W/m^2), K_i is the thermal conductivity of ice (J·m^{-1}·s^{-1}·K^{-1}), θ_b is the vertical basal ice temperature gradient (K/m), ρ_i is the ice density (kg/m^3), and L is the specific latent heat of fusion (J/kg).

2.2. Water Content of the Till Layer

Building on previous work (Christoffersen et al., 2014), we adopted an approach in which the water content in the till layer was estimated by linking basal traction from inversions with two specific material characteristics that describe the plastic rheology of the till. The first material characteristic is the aforementioned Coulomb plastic failure criterion, which prescribes the till's shear strength, τ_f (Pa), as a linear function of the effective normal stress, N (Pa):

$$\tau_f = N \tan\phi, \tag{2}$$

where $\phi = 24 \pm 0.3°$ is a constant value for the till's friction angle and cohesion is negligible (Tulaczyk et al., 2000a). Using this equation with the shear strength assumed to be equal to the inverted basal traction field, we further calculated the effective pressure in the till.

The second characteristic is the till's compressibility, which is described by a logarithmic function relating the till void ratio (e (ND), a quantity directly related to porosity), to the effective normal stress:

$$e = e_o - C \log\left(\frac{N}{N_o}\right), \tag{3}$$

where C is a constant for compressibility which has a relatively narrow range of values (0.12–0.15) when the till is normally consolidated, and e_o is the void ratio at the reference value of effective normal stress N_o (Tulaczyk et al., 2000a). By combining the two equations (equations (2) and (3)), we can eliminate N and specify the void ratio as a function of the till's yield strength:

$$e = -\frac{1}{b}\ln\left(\frac{\tau_f}{a}\right), \tag{4}$$

where τ_f is the shear strength (Pa) assumed to be equal to the basal traction τ_b derived from the numerical inversions, and $a = 944 \times 10^6$ Pa and $b = 21.7$ are empirical constants (Tulaczyk et al., 2000b).

Seismic surveys imply that most of the fast-flowing regions of PIG are underlain by a soft and deformable till (Brisbourne et al., 2017; Smith et al., 2013). The measured acoustic impedances suggest that the till there has a high porosity (30–45% beneath the trunk and tributaries and <30% in between the tributaries) and that its thickness ranges from 1.5 to 13 m beneath the trunk and tributaries, respectively. Assuming a normal distribution of the till thickness with these values as end-members, we obtained a characteristic till thickness $Z_s = 7.2 \pm 1.9$ m. With similar thickness ranges observed in troughs of tributaries T1 and T7 (6 to 10 m) and in the intertributary region between T5 and T7 (7 ± 3 m; Brisbourne et al., 2017), we simply prescribed the value of the characteristic till thickness uniformly throughout the modeled domain.

Estimates of subglacial water storage were obtained by multiplying the till layer thickness with the spatially varying distribution of pore water, quantified as the till void ratio e, as described above. The corresponding effective water layer thus became $W_{\text{till}} = eZ_s$ (in m). To estimate how much water left or entered the till layer, we calculated the change in effective water layer (ΔW_{till}, m), expressed with

$$\Delta W_{\text{till}} = \Delta e Z_s, \tag{5}$$

where Δe (ND) is the change in till void ratio between 1996 and 2014.

2.3. Regional Water Routing

We established the subglacial water pathways of PIG by specifying the hydrological sources and sinks at its bed and routing of water between them (Christoffersen et al., 2014). The sources include water rejected from the till layer in places where consolidation reduced the pore volumes between 1996 and 2014 ($\Delta W_{till} < 0$, equation (5)) as well as water produced by basal melting ($\dot{m}>0$). Sinks are defined as water that has entered the till layer in places where its porosity increased between 1996 and 2014, plus water that was consumed by basal freezing ($\dot{m}<0$). Thus, the distributed net rate of water production at the ice-till interface ($\dot{W}_{\text{net}}$, m/yr) is

$$\dot{W}_{\text{net}} = \dot{m} - \frac{\Delta W_{\text{till}}}{\Delta t}, \tag{6}$$

where $\dot{m}$ is the basal melt rate (m/yr) calculated from the numerical inversions (equation (1)), and Δt is the time period (yr) between observations made in 1996 and 2014.

Channelization of subglacial meltwater is an important aspect of ice dynamic in Antarctica (Carter et al., 2017; Damsgaard et al., 2017; Fricker et al., 2016; Horgan et al., 2013; Kamb, 2001; Le Brocq et al., 2013; Meyer et al., 2018; Winberry et al., 2009), and it is possible that water flows in concentrated channels beneath sections of PIG. Using a physically based model to assert the structure and nature of its drainage system is however beyond the scope of this study. In our simplified approach, the water is assumed to flow along the ice stream bed according to gradients in hydraulic potential, here calculated using a multiflow direction algorithm, where the flow is diverted to multiple downslope cells in proportion to the slope between them (Freeman, 1991; Quinn et al., 1991). In this work, the hydraulic potential surface (θ, Pa) is calculated over the same grid that specifies the ice flow model. In contrast to previous work (Carter & Fricker, 2012; Le Brocq et al., 2009), which assumed effective pressure to be constant or simply zero, we use the Coulomb plastic till approximation to derive the effective pressure from the spatially varying distribution of shear strength obtained with the model (equation (2)). Thus, we have

$$\theta = \rho_w g z_b + \rho_i g H - \frac{\tau_f}{\tan\phi}, \tag{7}$$

where ρ_w is the water density (kg/m^3), g is the constant of gravitational acceleration (m/s^2), z_b is the bed elevation (m), and H is the ice thickness (m).

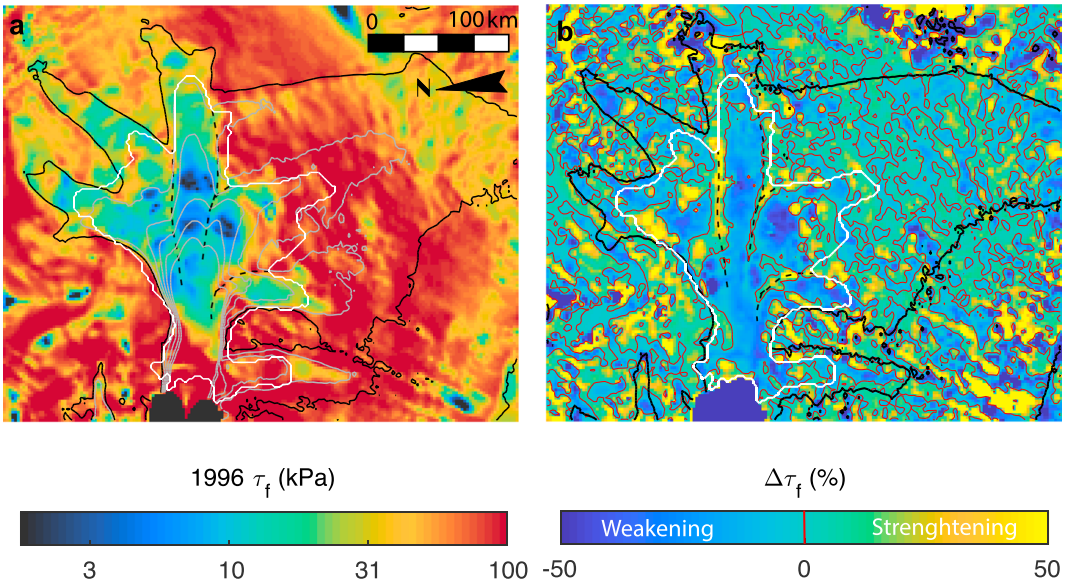

Figure 3. (a) Modeled basal stress distribution (kPa) from inversion of the 1996 surface velocity, overlain with the 50-m/yr velocity contour (black line) and the 100- to 500-m/yr velocity contours (gray lines with 100-m/yr spacing). The region of significant speed-up is outlined in white. The black-dashed lines identify zones of sticky spots coincident with shear margin location. (b) Distributed change in basal stress from 1996 to 2014 (%), overlain with the 0-value contour (red lines), the 50-m/yr velocity contour in 2014 (black line), and the region of significant speed-up (white contour). The black-dashed lines are as in (a).

3. Results

This study aims to establish how the subglacial environment of PIG changed between 1996 and 2014. Hence, we focus the majority of our analysis on the region that has experienced sufficient ice flow acceleration to infer changes taking place at the base of the glacier. Here we define "significant acceleration" to be an increase of at least 25 m/yr between 1996 and 2014 (Figure 2). This value delineates an area (henceforth "speed-up area") largely coincident with the region where fast (>100 m/yr) ice flow is induced by low (<50 kPa) basal resistance, conditions that underpin the Coulomb plastic bed approximation.

The first inversion run is referred to as I_{1996_MC}, where 1996 refers to the year of surface velocity observations and MC refers to the use of a glacier geometry obtained from mass conservation. The second inversion is referred to as $I_{2014\_\Delta H}$, where 2014 is the year of surface velocity observations while ΔH refers to the use of a geometry accounting for the observed recent ice thinning on PIG. To understand how the applied ice thinning affected our results, we also performed an inversion of the 2014 surface velocity using the geometry from mass conservation, identical to that used in the 1996 inversion. We refer to this inversion run as I_{2014_MC}.

Figure 2 shows PIG surface velocity observed in 2014, together with the observed and modeled velocity change since 1996. The spatial extent of acceleration is well captured, with a mean absolute modeled error of 13% over the whole domain and less (10%) when we consider the speed-up area only.

3.1. Modeled Changes in Basal Stress Between 1996 and 2014

The modeled basal stress distribution in 1996 (Figure 3a) shows an overall weak bed with little resistance to ice flow beneath the central trunk (τ_b~ <10 kPa) and tributaries (τ_b~10–30 kPa), with the exception of a strong pinning region spanning the whole width of the trunk just above the grounding line. The bed beneath the upper reaches of the southern tributaries (T1, T3, T5, and T7) is stronger (τ_b > 50 kPa). This result is in accordance with previous work (Gillet-Chaulet et al., 2016; Joughin et al., 2009; Morlighem et al., 2010) and suggests a transition from weak sediments to either consolidated sediments or hard bed. A close examination reveals elongated areas of relatively stronger bed within the fast trunk region (dashed lines in Figure 3), notably situated beneath shear margins identified from calculated strain rates (more details on these in

Table 1
Median and Quantiles [0.1 0.25 0.75 0.9] Values of Modeled Basal Stress for the 1996 and 2014 Inversions, and of Changes in Basal Stress, in Areas of Weakening

			Median $\Delta\tau_f$		
	Median τ_f (kPa)	Quantiles τ_f [0.1 0.25 0.75 0.9] (kPa)	kPa	%	Quantiles $\Delta\tau_f$ [0.1 0.25 0.75 0.9] (kPa)
I_{1996_MC}	20	[8 12 52 93]			
$I_{2014\_\Delta H}$	17	[6 10 44 83]	−2.8	−15	[−13 −6.5 −1.5 −0.7]

Note. Areas of weakening cover 64% of the speed-up region.

section 4.3). These areas were also identified in previous modeling studies where they were referred to as sticky spots (Gillet-Chaulet et al., 2016; Joughin et al., 2009; Sergienko & Hindmarsh, 2013).

We report changes in basal traction by calculating the median values of weakening and strengthening, with additional details on the spread of data given in Tables 1 and 2. Focusing on the speed-up area, we find that, between 1996 and 2014, 64% of PIG's bed has weakened, with modeled basal traction falling by 2.8 kPa (−15%; Table 1). The remaining 36% strengthened by 4.3 kPa (+12%; Figures 3b and 4a and Table 2). The distribution of the weakening and strengthening areas shown in Figure 3b is noteworthy, because strengthening concentrates near the ice stream shear margins, where the bed in 1996 was already comparatively stronger (32 kPa) than its surroundings (20 kPa; Tables 1 and 2). Thus, the weakest portions of the bed became even weaker, while the stronger portions became stronger (Figure 4a).

Because the applied thinning in the $I_{2014\_\Delta H}$ inversion may have influenced the basal stress by cooling of the steady-state ice temperature, we performed a sensitivity analysis using a separate inversion with no thinning applied (I_{2014_MC}). This showed that the applied change in geometry in the 2014 inversion cooled the mean temperature of the ice by just 0.3% (with a standard deviation of 0.8%), which means that this effect alone cannot explain the change in basal stress described above (Figure S2). We further show that differences in basal stress remain qualitatively similar to results presented above, when values of weakening and strengthening are calculated using a fixed geometry in the 2014 inversion (Tables S1 and S2 and see also Figure S3).

3.2. Modeled Changes in Basal Melting Between 1996 and 2014

The basal melt rate distribution calculated for the 1996 inversion (Figure 5a) is in good agreement with the previous findings of Joughin et al. (2009), with the exception of a few small areas of basal freezing where we instead calculate low rates of basal melting. A likely explanation for this is that Joughin et al. (2009) assume a constant geothermal heat flux value of 70 mW/m^2, which is lower than the spatially varying geothermal heat flux by Shapiro and Ritzwoller (2004) used in this study. The sensitivity of basal melting to values of geothermal heat flux is however low (1 mm/yr of melt increase per 10 mW/m^2) compared to the high-averaged melt rates calculated for this region (Joughin et al., 2009; Larour et al., 2012), which means that uncertainties in geothermal heat flux distribution should not affect our analysis. Indeed, we estimate the catchment-wide meltwater volume in 1996 to be 1.85 km^3/yr (or 59 m^3/s) which is similar to previous estimates (Joughin et al., 2009).

The basal meltwater production has, however, changed significantly since 1996, with the annual catchment-wide volume increasing by 25% to a total of 2.34 km^3/yr (74 m^3/s) in $I_{2014\_\Delta H}$ (Figures 5b and 5c). Within the speed-up region, we find basal melting to have increased nearly everywhere (>90% by area) and by an

Table 2
Median and Quantiles [0.1 0.25 0.75 0.9] Values of Modeled Basal Stress for the 1996 and 2014 Inversions, and of Changes in Basal Stress, in Areas of Strengthening

			Median $\Delta\tau_f$		
	Median τ_f (kPa)	Quantiles τ_f [0.1 0.25 0.75 0.9] (kPa)	kPa	%	Quantiles $\Delta\tau_f$ [0.1 0.25 0.75 0.9] (kPa)
I_{1996_MC}	32	[11 17 72 104]			
$I_{2014\_\Delta H}$	*37*	[13 20 85 116]	4.3	12	[0.5 1.4 9.1 17.5]

Note. Areas of strengthening cover 36% of the speed-up region.

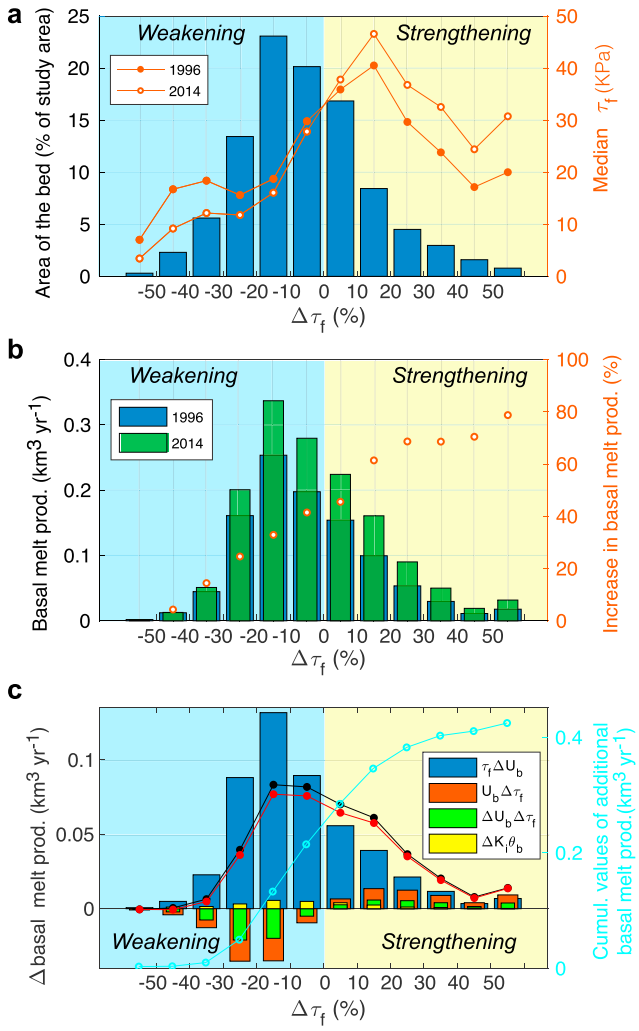

Figure 4. Analysis of changes in basal shear strength of Pine Island Glacier between 1996 and 2014. (a; left axis) Histogram with bins showing areas of the bed (% of the speed-up region) where basal drag τ_f increased and decreased (change in % labeled on the x axis). (right axis) Median value of basal drag (kPa, orange) in each bin for 1996 (solid dots) and 2014 (open circles). For example, the region where the bed strengthened by 10–20% covers 8.5% of the speed-up area and has a median value of τ_f equal to 40 kPa in 1996 and 46 kPa in 2014. (b; left axis) Same as (a) but with bins of histogram showing the annual basal melt volume produced (km^3/yr) in 1996 (blue bins) and 2014 (green bins). (right axis) Increase (%) in rates of basal melt production from 1996 to 2014 (open orange circles) in each bin, which indicates that increases in rates of basal melting are consistently higher where the bed strengthened. (c) Same as (a) and (b) but with bins partitioning changes in basal melt production stemming from (1) change in basal ice velocity (blue bins), (2) change in basal drag (orange bins), (3) simultaneous changes in basal velocity and drag (green bins), and (4) change in conductive heat loss (yellow bins). See equation (8) in text. Black line with solid dots show the total increase in melt production (km^3/yr) for each bin. Red line with solid dots show the increase in melt tied to changes in basal motion (sum of blue, orange, and green bins). The small difference between the black and red lines show that changes in basal velocity and/or drag are responsible for almost all of the additional basal melt produced in 2014. Cyan line with open circles shows the cumulative values for the increase in melt produced between 2014 and 1996 (right axis).

average of 28% (Figure 4b). We identify the processes responsible for this increase in the model, by rewriting equation (1) in terms of change over the 1996 to 2014 period:

$$\frac{\Delta\dot{m}}{\Delta t} = \frac{1}{L\rho_i\Delta t}(\tau_{b\_96}\Delta U_b + U_{b\_96}\Delta\tau_b + \Delta U_b\Delta\tau_b - K_i\Delta\theta_b + \Delta G). \quad (8)$$

The terms on the right-hand side partition the variation in basal melt rate due to changes in (1) basal velocity, (2) basal drag, (3) simultaneous changes in basal velocity and drag, (4) conductive heat loss, and (5) geothermal heat flux (here equal to 0, as the latter is fixed in the inversions). Results for terms 1–4 (Figure 4c) show that a higher frictional heat flux almost entirely explains the increase in basal melt production between 1996 and 2014, while changes in conductive heat loss are negligible. Although the observed speed-up over the 18-year period is associated with widespread basal weakening occurring over nearly two thirds of the bed in the speed-up region, our analysis reveals that only half of the additional melt volume is produced in such places of weaker basal strength (Figure 4c). The other half of the additional melt volume produced by 2014 is generated over the remaining one third of the speed-up region, principally near or at the glacier's shear margins where basal drag has increased (Figures 3 and 4c). Indeed, in such cases, the cumulative effect of increased basal traction and basal velocity leads to significant increases in rates of basal melt production between 1996 and 2014, in excess of 40% (Figure 4b).

3.3. Changes in Subglacial Till Water Content

When basal drag from inversions of ice flow is used as an estimate of till shear strength, we find that in 1996, till void ratios beneath PIG ranged from 0.38 to 0.64 (equation (4)). These void ratios correspond to porosities varying from 28% to 39%, which is in good agreement with the span of values (section 2.2) estimated from measured acoustic impedance (Brisbourne et al., 2017). Using the difference in basal drag between 1996 and 2014 as a means to estimate changes in till water storage (equation (5)), we find that flow of water into the till layer is around two orders of magnitude smaller than the volume of water produced by basal melting. Specifically, we calculate that the region of till weakening was associated with an intake of water amounting to 0.81 km^3, while the region of till strengthening rejected 0.38 km^3 of water into the assumed basal hydrological system (section 2.3) between 1996 and 2014.

3.4. Basal Hydrological Systems and Paths

To identify the first-order nature of the hydrological system beneath PIG, we routed water between sources and sinks at the ice stream base as described in section 2.3. Although the hydrological catchment extends farther than the interior limit of our domain, we do not prescribe additional water fluxes around the domain boundaries, as the water production outside our domain has been shown to be negligible compared to the production beneath the faster flowing ice (Joughin et al., 2009). Our analysis show an arborescent system of hydrological flow paths, unique within each tributary and the convergence into a single large concentrated path beneath the main trunk (Figure 6). We note in this context that the water routing does not show sensitivity to a doubling of the grid resolution (Figure S4). In addition, model testing indicates that the routing of water

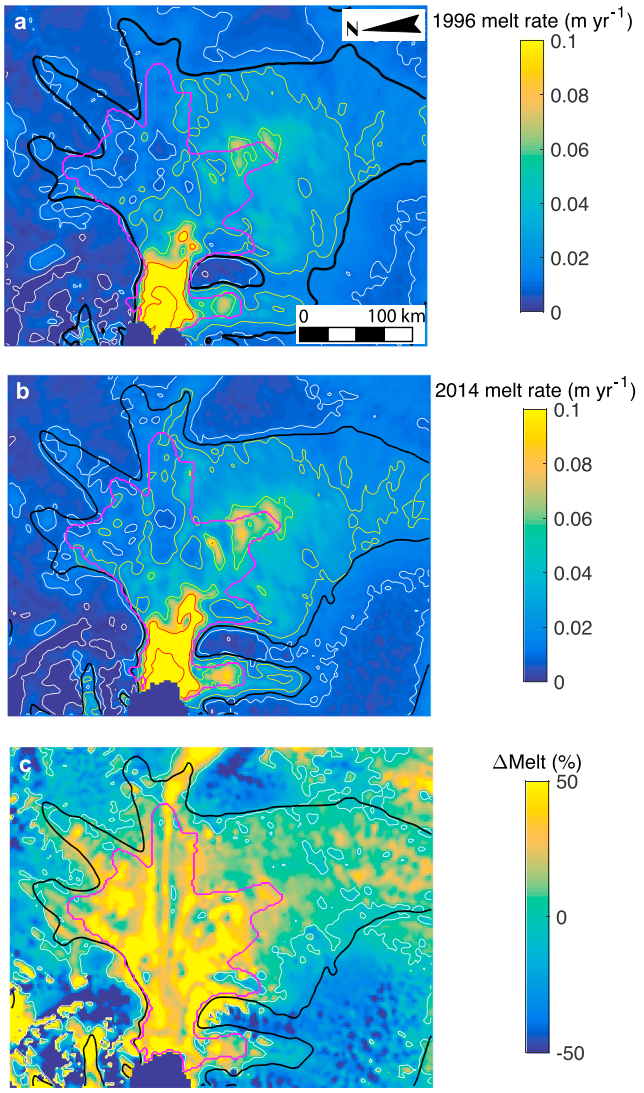

Figure 5. (a) Modeled map of basal melt rate (m/yr) from inversion of the 1996 surface velocity, overlain with the 50-m/yr velocity contour (black) and outline of the region of significant speed-up (magenta contour). We show the contours for melt values of 0.001–0.01 (white), 0.02–0.05 (yellow), and 0.1–0.5 m/yr (red). (b) As in (a) but showing basal melt from the inversion of the 2014 surface velocity. (c) Increase in basal melting production (%) from 1996 to 2014.

remains broadly similar (Figure S4), if we had assumed the effective pressure to be zero in equation (7).

Previous work has shown that changes in surface elevation can induce significant modifications of the direction of hydrological flow due to their effect on hydraulic potentials (Fischer et al., 2005; Karlsson & Dahl-Jensen, 2015; Wright et al., 2008). In line with these works, our model reveals that the surface elevation change that took place between 1996 and 2014 was sufficiently pronounced to alter the hydrological pathways beneath PIG tributaries. The most noticeable changes are modeled in the north sector, where tributaries T4 and T6 flow into the upper section of the main trunk (Figure 6b). We note that the bed in this sector is less topographically constrained than elsewhere in the domain, which facilitates rerouting of water (Wolovick et al., 2013), as the hydraulic potential surface becomes more sensitive to changes in surface elevation, or in effective pressure (Chu et al., 2016).

4. Discussion

Previous work has shown that the acceleration of PIG is linked to oceanographic forcing, with melting in the sub-ice-shelf cavity driving sustained retreat of the grounding line (Alley et al., 2015; Joughin et al., 2003, 2010; Mouginot et al., 2014; Park et al., 2013; Rignot et al., 2014; Shepherd et al., 2004), as well as inland thinning (Gillet-Chaulet et al., 2016; Scott et al., 2009). Our results show that evolving ice flow is also accompanied by significant changes in the magnitude and distribution of basal resistance (Figure 3b).

4.1. Ice-Till-Water Interaction in Regions of Significant Weakening

The widespread reduction of basal traction calculated across the speed-up region could be explained by increased porosity and additional storage of water in the basal till layer (Tulaczyk et al., 2000b). To investigate the extent to which regions of widespread basal weakening can be explained by direct incorporation of locally produced melt water into the till layer, we compared changes in local water storage with local melt rates from the inversions. To do so, we estimated the reduction of till strength during the period of observation based on the hypothesis that all basal melt water entered the till layer below. The corresponding expression for the 2014 melt-derived till strength (τ_{f14_melt}) is

$$\tau_{f14\_melt} = a\exp(-b(e_{96} + \Delta e)), \quad (9)$$

where e_{96} is the void ratio estimated from the 1996 inversion (equation (4)) and Δe is the increase in void ratio due to added melt water ($\Delta e = \frac{\dot{m}\times\Delta t}{Z_s}$, where $\dot{m}$ is taken as the mean of the distributed melt rates calculated in I_{1996_MC} and $I_{2014\_\Delta H}$).

In doing so, we can compare the distributed reduction in basal drag derived from the inversion ($\Delta\tau_{f\_inv} = \tau_{f14\_inv} - \tau_{f96\_inv}$) to an independently calculated weakening in till strength which assumes 18 years of continued basal melt water assimilation ($\Delta\tau_{f\_melt} = \tau_{f14\_melt} - \tau_{f96\_inv}$). Results are shown in Figure 7. The relationship between $\Delta\tau_{f\_inv}$ and $\Delta\tau_{f\_melt}$ is analyzed in a linear regression model, which indicates that just 40% (based on the coefficient of determination, $R^2 = 0.40$) of the weakening inferred from model inversions can be explained from direct assimilation of basal melt water into the till. However, when the regression is focused on the regions of the bed that experienced at least 15% weakening (red contour in

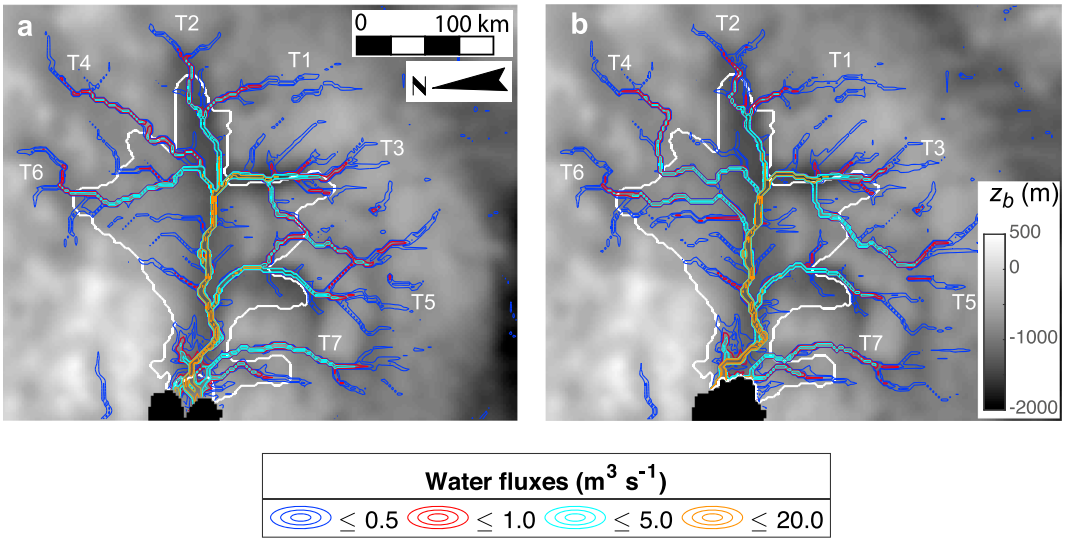

Figure 6. (a) Bed topography (z_b, m above sea level) overlain with subglacial water fluxes (in m^3/s), obtained from routing the distributed net rate of water production with melt rates calculated in the I_{1996_MC} inversion. The region of significant speed-up is outlined in white. The contours show fluxes up to 0.5 (blue), 1 (red), 5 (cyan), and 20 m^3/s (orange). The seven tributaries are labeled T1–T7. (b) As in (a) but for the $I_{2014\_\Delta H}$ inversion.

Figure 7), the regression model explains 75% ($R^2 = 0.75$) of the change in basal traction between 1996 and 2014 (Figure 7c). Areas not explained with the model include in particular the grounding line region, where melt rates are especially large due to fast flow. In equation (9), these translate into basal weakening significantly exceeding the weakening values calculated from inversions (Figure 7c). Although the till thickness distribution is poorly constrained, the regression outcome is not significantly sensitive to the value of Z_s assumed here. Indeed, the model explains 78% and 72% of the change in basal traction with respective values of till thickness set to their extrema of 1.5 and 13 m.

As seen in Figure 7, the second regression model covers 70% of the weakened bed of PIG and principally excludes marginal zones where there is a transition from bed weakening to strengthening in the model inversions. The higher coefficient of determination in the second regression model suggests that ice-till-water interactions and processes similar to those observed beneath the Siple Coast ice streams are the principal cause of the significant basal weakening that took place over large areas of PIG's bed between 1996 and 2014, in particular away from the grounding line. However, the first regression outcome implies that these processes are confined to central sectors of ice trunks and exclude zones closer to the margins (see also section 4.3).

4.2. Inferred Existence of an Efficient Hydrological System

Estimates of melt rates beneath PIG (averaging ~34 mm/yr in the speed-up region) are at least an order of magnitude larger than the basal melt rates estimated for the Siple Coast region (Bougamont et al., 2015; Joughin et al., 2004), and we estimate the volume of melt water produced by basal melting during this 18-year period to amount to 30 km^3 in the speed-up region. This is two orders of magnitude more than the volume of melt water accommodated into the till between 1996 and 2014 (section 3.3), which means that the water volume stored in the till layer is less significant in PIG's hydrological budget compared to the Siple Coast (Christoffersen et al., 2014). On the other hand, the large difference between melt water production and subglacial water storage supports the existence of an efficient hydrological system, without which large quantities of basal melt water could not be evacuated toward the grounding zone.

In the southern sector of PIG (T1, T3, T5, and T7) where the basal melt water production is high (Figures 5a and 5b), we find no significant change in the basal shear strength, suggesting that the water produced there has little or no impact on the physical bed properties. The relatively steep surface slopes in the southern region (Figure 1) may favor conditions that promote the development of concentrated channels that export

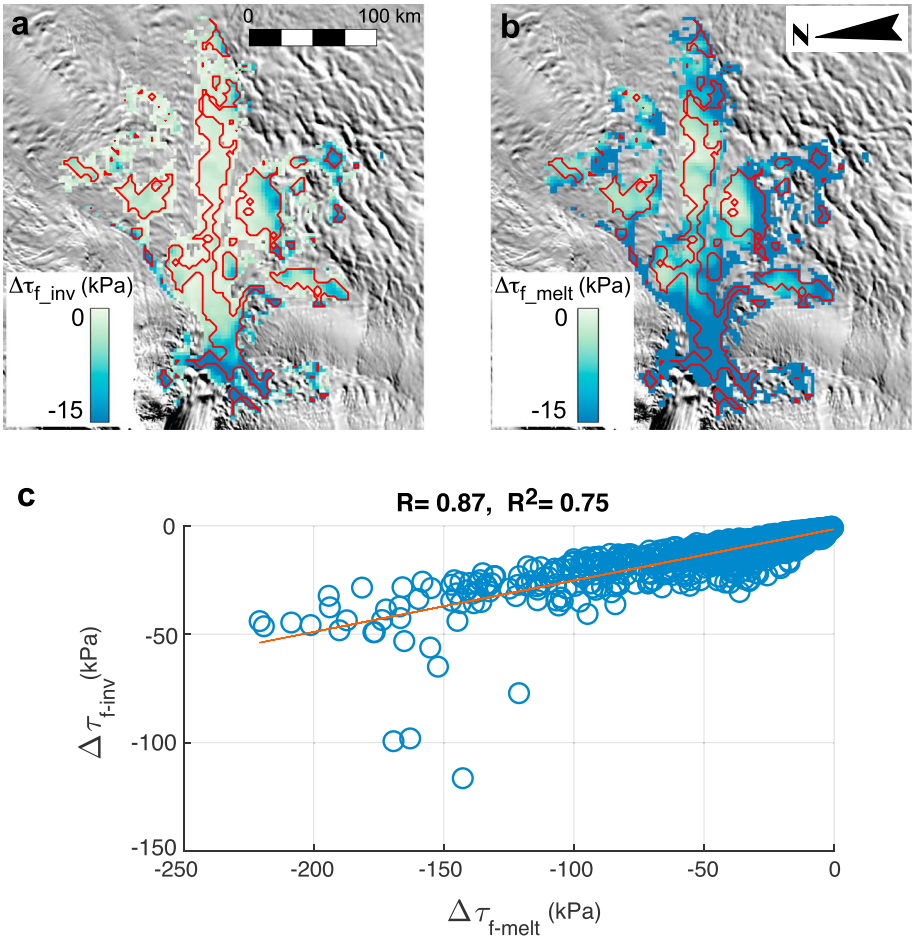

Figure 7. (a) Map of Pine Island Glacier showing basal weakening $\Delta\tau_{f\_inv}$ (kPa) derived from the difference between the basal drag calculated from inversions I_{1996_MC} and $I_{2014\_\Delta H}$. The red contour outlines regions of the bed that experienced at least 15% weakening. (b) Basal weakening $\Delta\tau_{f\_melt}$ (kPa) derived from the difference between the inverted 1996 basal drag and the 2014 basal drag calculated using equation (9). The red contour is as in (a). (c) Regression analysis between $\Delta\tau_{f\_inv}$ and $\Delta\tau_{f\_melt}$, focusing on regions of the bed that experienced at least 15% weakening. R is the correlation coefficient, and R^2 is the coefficient of determination.

water efficiently (Schroeder et al., 2013; Walder & Fowler, 1994). The existence and role of such channels beneath Antarctic glaciers are widely discussed in observation-based and modeling-based studies (Dow et al., 2018; Fricker et al., 2016; Kamb, 2001; Le Brocq et al., 2013; Meyer et al., 2018; Perol et al., 2015; Vogel et al., 2005). Here the presence of such channels is moreover consistent with the relatively high basal shear stress values estimated for this sector (this study; Joughin et al., 2009). We thus hypothesize that a channelized water system may be the dominant hydrological system in the southern sector of PIG.

4.3. Coincidence of Shear Margins, Channelized Flow, and Basal Strengthening

We identify shear margin positions from strain rates calculated along and across flow using the 1996 observed surface velocity map (Figure 8), noting that these positions are identical if the 2014 velocity map is used (Figure S5). Out of 15 identified shear margins (M1A-B to M7A-B, plus M5C), only five (M2A, M4A, M5C, M6A, and M6B) are topographically controlled, whereas six (M1A, M2B, M3A, M4B, M5A, and M7A) follow distinct pathways of the basal hydrological system in our model. For the remaining four shear margins (M1B, M3B, M5B, and M7B), we do not identify any distinct control in terms of topography, hydrology, or thermal conditions.

The shear margins that coalesce with basal melt water pathways are almost exclusively situated in the southern sector of PIG, where modeled basal melt rates are high, and the basal hydrological system is inferred to

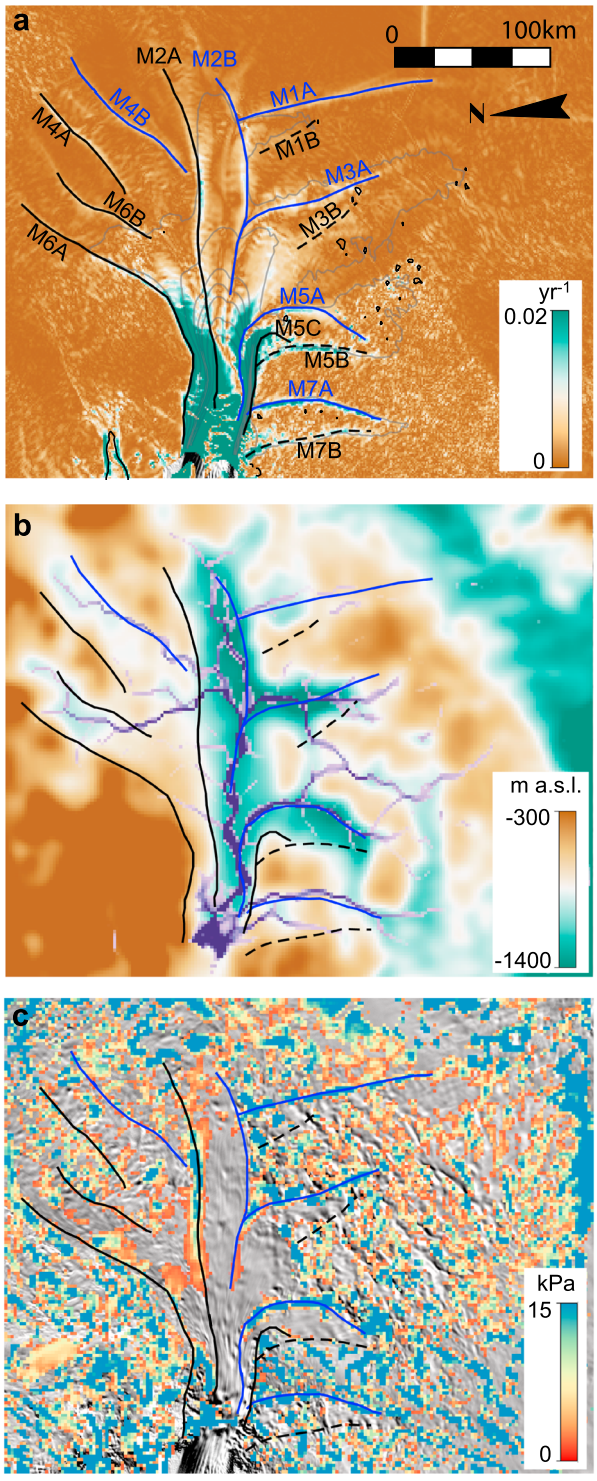

Figure 8. (a) Map of Pine Island Glacier showing shear strain rates (yr^{-1}) overlain with the 1996 velocity contours (gray, 200-m/yr increment) and identified shear margin location. We distinguish between topographically controlled margins (solid black), hydrologically controlled margins (solid blue), and margins showing no obvious control (dashed black). (b) Bed elevation (m above sea level) overlain with identified shear margins and hydrological water fluxes calculated from the I_{1996_MC} inversion. (c) Basal strengthening (kPa) between 1996 and 2014 calculated from the inversions and overlain with identified shear margins.

be composed of efficient channels (section 4.2). It is therefore possible that these shear margins formed in unison with a regional hydrological system that now locks them in place, as proposed in recent theoretical work (Elsworth & Suckale, 2016; Meyer et al., 2016; Perol et al., 2015; Platt et al., 2016). It has been suggested that high deformation rates along shear margins could result in relatively thick layers of temperate ice, which would impede conduction of heat away from the bed and generate high basal melt rates (Beem et al., 2010; Jacobson & Raymond, 1998; Perol et al., 2015; Raymond et al., 2001; Schoof, 2012; Suckale et al., 2014). With large volumes of water produced, efficient channels with low-water pressure may develop and draw additional water from their surroundings (Rothlisberger, 1972; Weertman, 1972), thereby strengthening the bed in a manner that is consistent with this study. Theoretically, these channels are capable of reducing the pore pressure along the bed over a distance of several kilometers, thus providing a mechanism to increase the local basal drag and stabilize the position of the margin when ice-flow acceleration increases the amount of shearing along the margin (Elsworth & Suckale, 2016; Meyer et al., 2016; Perol et al., 2015; Platt et al., 2016).

Although our model inversions do not feature designated shear margin processes, the basal conditions we derive nonetheless provide independent support to the theoretical characterization of shear margins detailed in previous work. The juxtaposition of shear margins and hydrological pathways beneath PIG is a striking output from our model, which is the first to show that strong portions of the bed along shear margins have become even stronger during a period of sustained ice-flow acceleration (Figures 3 and 4). Furthermore, the modeled basal strengthening along such margins (M1A, M3A, M5A, and M7A, Figure 8) ranges from 15 to 55 kPa (Figure S6) over the 18-year period, which is considerably more than the average strengthening of 4.3 kPa calculated for the entire speed-up area (section 3.1). It is possible that processes not included in our model would in reality influence the viscosity of ice and thereby influence basal drag in our model. However, with previous theoretical work showing formation of temperate ice due to high strain in shear margins, the omission of those processes should mean that the increase in basal drag between 1997 and 2014 could in fact be even larger than what our results suggest. Moreover, with several margins (e.g., M5B, M5C, and M7B) showing high strain rates but no significant change in basal traction over time, it is unlikely that changes along margins M1A, M3A, M5A, and M7A are merely an artifact of simplified physics in our model. Given that the reported increase in basal drag often occurs along subglacial drainage pathways, we propose that the modeled basal strengthening might be a direct result of hydrological processes associated with efficient hydrology and high basal water fluxes, an interpretation which is consistent with previous work (Platt et al., 2016; Schroeder et al., 2013).

Hydrologically induced strengthening also provides a viable explanation for our model output along margin M2A (located along the northern edge of PIG's central trough), where inversions show basal traction and melt rates simultaneously increasing during the period of observations (Figures 3b and 5c). As our inversions show particularly significant increases in basal traction between 1996 and 2014 (Figure 8c), the theoretical considerations described above would imply that channels also exist there, notwithstanding that this margin is positioned outside the main paths of the regional hydrological system. Because those channels do

not coincide with hydrological lows, they cannot appear in the steady-state routing applied in this study (Figure 8b). Previous theoretical work has, however, shown that melting of ice along shear margins occur at sufficiently high rates to explain the formation of efficient channels. We speculate that hydrologically controlled shear margins may form two distinct groups. The first group are margins that may have evolved in unison with a regional hydrological system that now locks them in place. The second group are margins of different nature (e.g., topographical), which subsequently became locked in place by their local hydrological setting.

All of the southern shear margins associated with basal hydrology appear to be distinctly coupled with a margin for which no control can be identified (black-dashed lines in Figure 8). While speculative, it is possible that margins locked in place by hydrology exert control on those that are not. Analysis of airborne radio-echo sounding data points to the possible past migration of some of these margins, including margins of T3 and the western margin of T7 (Karlsson et al., 2009). Without sufficient topographical confinement or thermal boundary conditions, the overall mechanisms responsible for such migration are still uncertain (Platt et al., 2016; Raymond et al., 2001; Schoof, 2004), although one recent study (Kyrke-Smith et al., 2015) suggested that the width and spacing of ice streams may be defined with a natural length-scale resulting from the distribution of meltwater and effective pressure at the bed.

5. Summary and Conclusions

A large and growing body of evidence has tied the origin of sustained acceleration of PIG to its interaction with the ocean (Joughin et al., 2016; Konrad et al., 2017; Rignot et al., 2014). While previous work have characterized the physical state of the bed (Bingham et al., 2017; Brisbourne et al., 2017; Rippin et al., 2011; Smith et al., 2013; Vaughan et al., 2006) and tested its representation in numerical models (Gillet-Chaulet et al., 2016; Joughin et al., 2009, 2010; Morlighem et al., 2010; Sergienko & Hindmarsh, 2013; Vieli & Payne, 2003), no study so far has investigated how basal properties have evolved over time. In this study, we specifically address how basal properties of PIG changed between 1996 and 2014 when the glacier experienced sustained acceleration. Using inverse modeling, we show that flow acceleration and dynamic thinning was accompanied by pervasive changes in the basal environment, from which we infer the existence of two hydrological regimes (i.e., local exchanges with the till layer and the regional transport of water in efficient channels), as summarized below.

Overall, we find that the availability of basal water has increased by 25% between 1996 and 2014 and that the basal drag dropped by 15% on average over an area corresponding to two thirds of the speed-up region. We propose that this weakening was a direct response to the incorporation of locally produced basal melt water into an underling till layer. With weak portions of the bed becoming weaker subsequent to the glacier's interaction with the ocean, this loss of basal traction may have contributed further to the glacier's acceleration (Joughin et al., 2010, 2014).

This study also reveals significant ongoing strengthening of shear margins. This is an important, but so far overlooked mechanism for PIG, as it partially offsets the widespread reduction of basal resistance. We report this strengthening of shear margins, not just at the onset of fast flow, but also within the fast-flowing main trunk of PIG. Our findings indicate that large volumes of basal melt water may be produced along shear margins, and we hypothesize that the evacuation of this water along the bed may take place in low-pressure channels. Tentatively, the channels may have become larger and even more effective when PIG accelerated, thereby strengthening the surrounding bed. The future flow of PIG may thus be significantly influenced by a coevolution of basal properties and shear margins in addition to the glacier's interaction with the ocean. With water produced abundantly beneath PIG, we speculate that the hydrological control on shear margins may be strong in this region.

The extent to which Antarctic ice streams and glaciers will either retreat indefinitely (“collapse”) or find a new equilibrium state in response to future oceanic forcing of ice shelves may thus rest on processes involving subglacial hydrological processes not currently implemented in numerical ice sheet models that lead to positive as well as negative feedbacks. With PIG currently responsible for 20% of the West Antarctic contribution to sea level rise, it is crucial to develop a complete understanding all of the processes and mechanisms that sustain and restrain its fast flow to accurately project sea-level rise.

Acknowledgments
This work was funded by the Natural Environment Research Council (NERC) iSTAR programme (NE/J005800/1, NE/J005738, and NE/J005754/1) and the Isaac Newton Trust. The numerical code can be downloaded from https://cism.github.io. The mass conserved geometry required to replicate this work is available to download from the UK Polar Data Centre's Discovery Metadata System (http://doi.org/cj88) and the observed velocity from Enveo (http://cryoportal.enveo.at). The model output presented is available to download from the UK Polar Data Centre's Discovery Metadata System (https://doi.org/ct8b). We are grateful to the Editor, Associate Editor, and three anonymous reviewers for their helpful comments.

References

Alley, R. B., Anandakrishnan, S., Christianson, K., Horgan, H. J., Muto, A., Parizek, B. R., et al. (2015). Oceanic forcing of ice-sheet retreat: West Antarctica and more. In R. Jeanloz & K. H. Freeman (Eds.). *Annual Review of Earth and Planetary Sciences*, *43*, 207–231.

Alley, R. B., Blankenship, D. D., Bentley, C. R., & Rooney, S. T. (1986). Deformation of till beneath ice stream-B, West Antarctica. *Nature*, *322*(6074), 57–59. https://doi.org/10.1038/322057a0

Anandakrishnan, S. (2003). Dilatant till layer near the onset of streaming flow of ice stream C, West Antarctica, determined by AVO (amplitude vs offset) analysis. *Annals of Glaciology*, *36*, 283–286.

Beem, L. H., Jezek, K. C., & Van der Veen, C. J. (2010). Basal melt rates beneath Whillans Ice Stream, West Antarctica. *Journal of Glaciology*, *56*(198), 647–654. https://doi.org/10.3189/002214310793146241

Beem, L. H., Tulaczyk, S. M., King, M. A., Bougamont, M., Fricker, H. A., & Christoffersen, P. (2014). Variable deceleration of Whillans Ice Stream, West Antarctica. *Journal of Geophysical Research: Earth Surface*, *119*, 212–224. https://doi.org/10.1002/2013jf002958

Bingham, R. G., Vaughan, D. G., King, E. C., Davies, D., Cornford, S. L., Smith, A. M., et al. (2017). Diverse landscapes beneath Pine Island Glacier influence ice flow. *Nature Communications*, *8*(1), 1618. https://doi.org/10.1038/s41467-017-01597-y

Bougamont, M., Christoffersen, P., Hubbard, A. L., Fitzpatrick, A. A., Doyle, S. H., & Carter, S. P. (2014). Sensitive response of the Greenland ice sheet to surface melt drainage over a soft bed. *Nature Communications*, *5*(1). https://doi.org/10.1038/ncomms6052

Bougamont, M., Christoffersen, P., Price, S. F., Fricker, H. A., Tulaczyk, S., & Carter, S. P. (2015). Reactivation of Kamb Ice Stream tributaries triggers century-scale reorganization of Siple Coast ice flow in West Antarctica. *Geophysical Research Letters*, *42*, 8471–8480. https://doi.org/10.1002/2015GL065782

Brisbourne, A. M., Smith, A. M., Vaughan, D. G., King, E. C., Davies, D., Bingham, R. G., et al. (2017). Bed conditions of Pine Island Glacier, West Antarctica. *Journal of Geophysical Research: Earth Surface*, *122*, 419–433. https://doi.org/10.1002/2016JF004033

Carter, S. P., & Fricker, H. A. (2012). The supply of subglacial meltwater to the grounding line of the Siple Coast, West Antarctica. *Annals of Glaciology*, *53*(60), 267–280. https://doi.org/10.3189/2012AoG60A119

Carter, S. P., Fricker, H. A., & Siegfried, M. R. (2017). Antarctic subglacial lakes drain through sediment-floored canals: Theory and model testing on real and idealized domains. *The Cryosphere*, *11*(1), 381–405. https://doi.org/10.5194/tc-11-381-2017

Christoffersen, P., Bougamont, M., Carter, S. P., Fricker, H. A., & Tulaczyk, S. (2014). Significant groundwater contribution to Antarctic ice streams hydrologic budget. *Geophysical Research Letters*, *41*, 2003–2010. https://doi.org/10.1002/2014GL059250

Christoffersen, P., & Tulaczyk, S. (2003). Response of subglacial sediments to basal freeze-on—1. Theory and comparison to observations from beneath the West Antarctic Ice Sheet. *Journal of Geophysical Research*, *108*(B4), 2222. https://doi.org/10.1029/2002JB001935

Chu, W., Creyts, T. T., & Bell, R. E. (2016). Rerouting of subglacial water flow between neighboring glaciers in West Greenland. *Journal of Geophysical Research: Earth Surface*, *121*, 925–938. https://doi.org/10.1002/2015JF003705

Comiso, J. C. (2000). Variability and trends in Antarctic surface temperatures from in situ and satellite infrared measurements. *Journal of Climate*, *13*(10), 1674–1696. https://doi.org/10.1175/1520-0442(2000)013<1674:vatias>2.0.co;2

Cornford, S. L., Martin, D. F., Payne, A. J., Ng, E. G., Le Brocq, A. M., Gladstone, R. M., et al. (2015). Century-scale simulations of the response of the West Antarctic Ice Sheet to a warming climate. *The Cryosphere*, *9*(4), 1579–1600. https://doi.org/10.5194/tc-9-1579-2015

Crabtree, D. R., & Doake, C. S. M. (1982). Pine Island Glacier and its drainage basin: Results from radio echo-sounding. *Annals of Glaciology*, *3*, 65–70. https://doi.org/10.1017/S0260305500002548

Damsgaard, A., Suckale, J., Piotrowski, J. A., Houssais, M., Siegfried, M. R., & Fricker, H. A. (2017). Sediment behavior controls equilibrium width of subglacial channels. *Journal of Glaciology*, *63*(242), 1034–1048. https://doi.org/10.1017/jog.2017.71

De Rydt, J., & Gudmundsson, G. H. (2016). Coupled ice shelf-ocean modeling and complex grounding line retreat from a seabed ridge. *Journal of Geophysical Research: Earth Surface*, *121*, 865–880. https://doi.org/10.1002/2015JF003791

DeConto, R. M., & Pollard, D. (2016). Contribution of Antarctica to past and future sea-level rise. *Nature*, *531*(7596), 591–597. https://doi.org/10.1038/nature17145

Dow, C. F., Werder, M. A., Babonis, G., Nowicki, S., Walker, R. T., Csatho, B., & Morlighem, M. (2018). Dynamics of active subglacial lakes in recovery ice stream. *Journal of Geophysical Research: Earth Surface*, *123*, 837–850. https://doi.org/10.1002/2017JF004409

Dukowicz, J. K., Price, S. F., & Lipscomb, W. H. (2010). Consistent approximations and boundary conditions for ice-sheet dynamics from a principle of least action. *Journal of Glaciology*, *56*(197), 480–496. https://doi.org/10.3189/002214310792447851

Dutrieux, P., De Rydt, J., Jenkins, A., Holland, P. R., Ha, H. K., Lee, S. H., et al. (2014). Strong sensitivity of Pine Island ice-shelf melting to climatic variability. *Science*, *343*(6167), 174–178. https://doi.org/10.1126/science.1244341

Elsworth, C. W., & Suckale, J. (2016). Rapid ice flow rearrangement induced by subglacial drainage in West Antarctica. *Geophysical Research Letters*, *43*, 11,697–11,707. https://doi.org/10.1002/2016GL070430

Engelhardt, H., & Kamb, B. (1998). Basal sliding of ice stream B, West Antarctica. *Journal of Glaciology*, *44*(147), 223–230.

Favier, L., Durand, G., Cornford, S. L., Gudmundsson, G. H., Gagliardini, O., Gillet-Chaulet, F., et al. (2014). Retreat of Pine Island Glacier controlled by marine ice-sheet instability. *Nature Climate Change*, *4*(2), 117–121. https://doi.org/10.1038/nclimate2094

Fischer, U. H., Braun, A., Bauder, A., & Flowers, G. E. (2005). Changes in geometry and subglacial drainage derived from digital elevation models: Unteraargletscher, Switzerland, 1927–1997. *Annals of Glaciology*, *40*, 20–24. https://doi.org/10.3189/172756405781813528

Flament, T., & Remy, F. (2012). Dynamic thinning of Antarctic glaciers from along-track repeat radar altimetry. *Journal of Glaciology*, *58*(211), 830–840. https://doi.org/10.3189/2012JoG11J118

Freeman, T. G. (1991). Calculating catchment-area with divergent flow based on a regular grid. *Computers & Geosciences*, *17*(3), 413–422. https://doi.org/10.1016/0098-3004(91)90048-i

Fretwell, P., Pritchard, H. D., Vaughan, D. G., Bamber, J. L., Barrand, N. E., Bell, R., et al. (2013). Bedmap2: Improved ice bed, surface and thickness datasets for Antarctica. *The Cryosphere*, *7*(1), 375–393. https://doi.org/10.5194/tc-7-375-2013

Fricker, H. A., Siegfried, M. R., Carter, S. P., & Scambos, T. A. (2016). A decade of progress in observing and modelling Antarctic subglacial water systems. *Philosophical Transactions of the Royal Society a-Mathematical Physical and Engineering Sciences*, *374*(2059). https://doi.org/10.1098/rsta.2014.0294

Gasson, E., DeConto, R. M., Pollard, D., & Levy, R. H. (2016). Dynamic Antarctic ice sheet during the early to mid-Miocene. *Proceedings of the National Academy of Sciences of the United States of America*, *113*(13), 3459–3464. https://doi.org/10.1073/pnas.1516130113

Gillet-Chaulet, F., Durand, G., Gagliardini, O., Mosbeux, C., Mouginot, J., Remy, F., & Ritz, C. (2016). Assimilation of surface velocities acquired between 1996 and 2010 to constrain the form of the basal friction law under Pine Island Glacier. *Geophysical Research Letters*, *43*, 10,311–10,321. https://doi.org/10.1002/2016GL069937

Gladstone, R. M., Lee, V., Rougier, J., Payne, A. J., Hellmer, H., Le Brocq, A., et al. (2012). Calibrated prediction of Pine Island Glacier retreat during the 21st and 22nd centuries with a coupled flowline model. *Earth and Planetary Science Letters*, *333–334*, 191–199. https://doi.org/10.1016/j.epsl.2012.04.022

Goldberg, D. N., Little, C. M., Sergienko, O. V., Gnanadesikan, A., Hallberg, R., & Oppenheimer, M. (2012). Investigation of land ice-ocean interaction with a fully coupled ice-ocean model: 2. Sensitivity to external forcings. *Journal of Geophysical Research*, *117*, F02038. https://doi.org/10.1029/2011JF002247

Horgan, H. J., Alley, R. B., Christianson, K., Jacobel, R. W., Anandakrishnan, S., Muto, A., et al. (2013). Estuaries beneath ice sheets. *Geology*, *41*(11), 1159–1162. https://doi.org/10.1130/G34654.1

Jacobs, S. S., Hellmer, H. H., & Jenkins, A. (1996). Antarctic ice sheet melting in the Southeast Pacific. *Geophysical Research Letters*, *23*, 957–960. https://doi.org/10.1029/96GL00723

Jacobs, S. S., Jenkins, A., Giulivi, C. F., & Dutrieux, P. (2011). Stronger ocean circulation and increased melting under Pine Island Glacier ice shelf. *Nature Geoscience*, *4*(8), 519–523. https://doi.org/10.1038/ngeo1188

Jacobson, H. P., & Raymond, C. F. (1998). Thermal effects on the location of ice stream margins. *Journal of Geophysical Research*, *103*, 12,111–12,122. https://doi.org/10.1029/98JB00574

Jamieson, S. S. R., Vieli, A., Livingstone, S. J., Cofaigh, C. O., Stokes, C., Hillenbrand, C. D., & Dowdeswell, J. A. (2012). Ice-stream stability on a reverse bed slope. *Nature Geoscience*, *5*(11), 799–802. https://doi.org/10.1038/ngeo1600

Jenkins, A., Dutrieux, P., Jacobs, S. S., McPhail, S. D., Perrett, J. R., Webb, A. T., & White, D. (2010). Observations beneath Pine Island Glacier in West Antarctica and implications for its retreat. *Nature Geoscience*, *3*(7), 468–472. https://doi.org/10.1038/ngeo890

Joughin, I., Rignot, E., Rosanova, C. E., Lucchitta, B. K., & Bohlander, J. (2003). Timing of recent accelerations of Pine Island Glacier, Antarctica. *Geophysical Research Letters*, *30*(13), 1706. https://doi.org/10.1029/2003GL017609

Joughin, I., Shean, D. E., Smith, B. E., & Dutrieux, P. (2016). Grounding line variability and subglacial lake drainage on Pine Island Glacier, Antarctica. *Geophysical Research Letters*, *43*, 9093–9102. https://doi.org/10.1002/2016GL070259

Joughin, I., Smith, B. E., & Holland, D. M. (2010). Sensitivity of 21st century sea level to ocean-induced thinning of Pine Island Glacier, Antarctica. *Geophysical Research Letters*, *37*, L20502. https://doi.org/10.1029/2010GL044819

Joughin, I., Smith, B. E., & Medley, B. (2014). Marine ice sheet collapse potentially under way for the Thwaites Glacier Basin, West Antarctica. *Science*, *344*(6185), 735–738. https://doi.org/10.1126/science.1249055

Joughin, I., Tulaczyk, S., Bamber, J. L., Blankenship, D., Holt, J. W., Scambos, T., & Vaughan, D. G. (2009). Basal conditions for Pine Island and Thwaites Glaciers, West Antarctica, determined using satellite and airborne data. *Journal of Glaciology*, *55*(190), 245–257. https://doi.org/10.3189/002214309788608705

Joughin, I., Tulaczyk, S., MacAyeal, D. R., & Engelhardt, H. (2004). Melting and freezing beneath the Ross ice streams, Antarctica. *Journal of Glaciology*, *50*(168), 96–108. https://doi.org/10.3189/172756504781830295

Kamb, B. (1991). Rheological nonlinearity and flow instability in the deforming bed mechanism of ice stream motion. *Journal of Geophysical Research*, *96*, 16,585–16,595. https://doi.org/10.1029/91JB00946

Kamb, B. (2001). Basal zone of the West Antarctic ice streams and its role in lubrication of their rapid motion. In R. B. Alley, & R. A. Bindschadler (Eds.), *The West Antarctic Ice Sheet: Behavior and Environment* (Vol. 77, pp. 157–201).

Karlsson, N. B., & Dahl-Jensen, D. (2015). Response of the large-scale subglacial drainage system of Northeast Greenland to surface elevation changes. *The Cryosphere*, *9*(4), 1465–1479. https://doi.org/10.5194/tc-9-1465-2015

Karlsson, N. B., Rippin, D. M., Vaughan, D. G., & Corr, H. F. J. (2009). The internal layering of Pine Island Glacier, West Antarctica, from airborne radar-sounding data. *Annals of Glaciology*, *50*(51), 141–146. https://doi.org/10.3189/s0260305500250660

Konrad, H., Gilbert, L., Cornford, S. L., Payne, A., Hogg, A., Muir, A., & Shepherd, A. (2017). Uneven onset and pace of ice-dynamical imbalance in the Amundsen Sea Embayment, West Antarctica. *Geophysical Research Letters*, *44*, 910–918. https://doi.org/10.1002/2016GL070733

Kyrke-Smith, T. M., Katz, R. F., & Fowler, A. C. (2015). Subglacial hydrology as a control on emergence, scale, and spacing of ice streams. *Journal of Geophysical Research: Earth Surface*, *120*, 1501–1514. https://doi.org/10.1002/2015JF003505

Larour, E., Morlighem, M., Seroussi, H., Schiermeier, J., & Rignot, E. (2012). Ice flow sensitivity to geothermal heat flux of Pine Island Glacier, Antarctica. *Journal of Geophysical Research*, *117*, F04023. https://doi.org/10.1029/2012JF002371

Le Brocq, A. M., Payne, A. J., Siegert, M. J., & Alley, R. B. (2009). A subglacial water-flow model for West Antarctica. *Journal of Glaciology*, *55*(193), 879–888. https://doi.org/10.3189/002214309790152564

Le Brocq, A. M., Ross, N., Griggs, J. A., Bingham, R. G., Corr, H. F. J., Ferraccioli, F., et al. (2013). Evidence from ice shelves for channelized meltwater flow beneath the Antarctic Ice Sheet. *Nature Geoscience*, *6*(11), 945–948. https://doi.org/10.1038/ngeo1977

Medley, B., Joughin, I., Smith, B. E., Das, S. B., Steig, E. J., Conway, H., et al. (2014). Constraining the recent mass balance of Pine Island and Thwaites Glaciers, West Antarctica, with airborne observations of snow accumulation. *The Cryosphere*, *8*(4), 1375–1392. https://doi.org/10.5194/tc-8-1375-2014

Meyer, C. R., Fernandes, M. C., Creyts, T. T., & Rice, J. R. (2016). Effects of ice deformation on Röthlisberger channels and implications for transitions in subglacial hydrology. *Journal of Glaciology*, *62*(234), 750–762. https://doi.org/10.1017/jog.2016.65

Meyer, C. R., Yehya, A., Minchew, B., & Rice, J. R. (2018). A model for the downstream evolution of temperate ice and subglacial hydrology along ice stream shear margins. *Journal of Geophysical Research: Earth Surface*, *123*, 1682–1698. https://doi.org/10.1029/2018JF004669

Morlighem, M., Rignot, E., Seroussi, H., Larour, E., Ben Dhia, H., & Aubry, D. (2010). Spatial patterns of basal drag inferred using control methods from a full-Stokes and simpler models for Pine Island Glacier, West Antarctica. *Geophysical Research Letters*, *37*, L14502. https://doi.org/10.1029/2010GL043853

Mouginot, J., Rignot, E., & Scheuchl, B. (2014). Sustained increase in ice discharge from the Amundsen Sea Embayment, West Antarctica, from1973 to 2013. *Geophysical Research Letters*, *41*, 1576–1584. https://doi.org/10.1002/2013GL059069

Nagler, T., Rott, H., Hetzenecker, M., Wuite, J., & Potin, P. (2015). The Sentinel-1 Mission: New opportunities for ice sheet observations. *Remote Sensing*, *7*, 9371–9389. https://doi.org/10.3390/rs70709371

Nias, I. J., Cornford, S. L., & Payne, A. (2018). New mass-conserving bedrock topography for Pine Island Glacier impacts simulated decadal rates of mass loss. *Geophysical Research Letters*, *45*, 3173–3181. https://doi.org/10.1002/2017GL076493

Parizek, B. R., Christianson, K., Anandakrishnan, S., Alley, R. B., Walker, R. T., Edwards, R. A., et al. (2013). Dynamic (in) stability of Thwaites Glacier, West Antarctica. *Journal of Geophysical Research: Earth Surface*, *118*, 638–655. https://doi.org/10.1002/jgrf.20044

Park, J. W., Gourmelen, N., Shepherd, A., Kim, S. W., Vaughan, D. G., & Wingham, D. J. (2013). Sustained retreat of the Pine Island Glacier. *Geophysical Research Letters*, *40*, 2137–2142. https://doi.org/10.1002/grl.50379

Pattyn, F. (2003). A new three-dimensional higher-order thermomechanical ice sheet model: Basic sensitivity, ice stream development, and ice flow across subglacial lakes. *Journal of Geophysical Research*, *108*(B8), 2382. https://doi.org/10.1029/2002JB002329

Payne, A. J., Vieli, A., Shepherd, A. P., Wingham, D. J., & Rignot, E. (2004). Recent dramatic thinning of largest West Antarctic ice stream triggered by oceans. *Geophysical Research Letters*, *31*, L23401. https://doi.org/10.1029/2004GL021284

Perol, T., Rice, J. R., Platt, J. D., & Suckale, J. (2015). Subglacial hydrology and ice stream margin locations. *Journal of Geophysical Research: Earth Surface*, *120*, 1352–1368. https://doi.org/10.1002/2015JF003542

Platt, J. D., Perol, T., Suckale, J., & Rice, J. R. (2016). Determining conditions that allow a shear margin to coincide with a Rothlisberger channel. *Journal of Geophysical Research: Earth Surface*, *121*, 1273–1294. https://doi.org/10.1002/2015JF003707

Pollard, D., & DeConto, R. M. (2009). Modelling West Antarctic ice sheet growth and collapse through the past five million years. *Nature*, *458*(7236), 329–332. https://doi.org/10.1038/nature07809

Price, S., Lipscomb, W. H., Hoffman, M., Hagdorn, M., Payne, A., Hebeler, F., & Kennedy, J. H. (2015). Community Ice Sheet Model (CISM) v2.0.5 documentation, Los Alamos, NM. [online] Available from: http://oceans11.lanl.gov/cism/data/cism_documentation_v2.0.pdf.

Price, S. F., Hoffman, M. J., Bonin, J. A., Howat, I. M., Neumann, T., Saba, J., et al. (2017). An ice sheet model validation framework for the Greenland ice sheet. *Geoscientific Model Development*, *10*(1), 255–270. https://doi.org/10.5194/gmd-10-255-2017

Price, S. F., Payne, A. J., Howat, I. M., & Smith, B. E. (2011). Committed sea-level rise for the next century from Greenland ice sheet dynamics during the past decade. *Proceedings of the National Academy of Sciences of the United States of America*, *108*(22), 8978–8983. https://doi.org/10.1073/pnas.1017313108

Quinn, P., Beven, K., Chevallier, P., & Planchon, O. (1991). The prediction of hillslope flow paths for distributed hydrological modeling using digital terrain models. *Hydrological Processes*, *5*(1), 59–79. https://doi.org/10.1002/hyp.3360050106

Raymond, C. F., Echelmeyer, K. A., Whillans, I. M., & Doake, C. S. M. (2001). Ice stream shear margins. In R. B. Alley & R. A. Bindschadler (Eds.), *The West Antarctic Ice Sheet: Behavior and environment* (Vol. 77, pp. 137-156), American Geophysical Union, Washington DC.

Retzlaff, R., & Bentley, C. R. (1993). Timing of stagnation of ice stream-C, West Antarctica, from short-pulse radar studies of buried surface crevasses. *Journal of Glaciology*, *39*(133), 553–561. https://doi.org/10.1017/S0022143000016440

Rignot, E., Mouginot, J., Morlighem, M., Seroussi, H., & Scheuchl, B. (2014). Widespread, rapid grounding line retreat of Pine Island, Thwaites, Smith, and Kohler Glaciers, West Antarctica, from 1992 to 2011. *Geophysical Research Letters*, *41*, 3502–3509. https://doi.org/10.1002/2014GL060140

Rignot, E., Mouginot, J., & Scheuchl, B. (2011). Antarctic grounding line mapping from differential satellite radar interferometry. *Geophysical Research Letters*, *38*, L10504. https://doi.org/10.1029/2011GL047109

Rignot, E., Velicogna, I., Van Den Broeke, M. R., Monaghan, A., & Lenaerts, J. (2011). Acceleration of the contribution of the Greenland and Antarctic ice sheets to sea level rise. *Geophysical Research Letters*, *38*, L05503. https://doi.org/10.1029/2011GL046583

Rippin, D. M., Vaughan, D. G., & Corr, H. F. J. (2011). The basal roughness of Pine Island Glacier, West Antarctica. *Journal of Glaciology*, *57*(201), 67–76. https://doi.org/10.3189/002214311795306574

Rothlisberger, H. (1972). Water pressure in intra- and subglacial channels. *Journal of Glaciology*, *11*(62), 177–203. https://doi.org/10.1017/S0022143000022188

Schoof, C. (2004). On the mechanics of ice-stream shear margins. *Journal of Glaciology*, *50*(169), 208–218. https://doi.org/10.3189/172756504781830024

Schoof, C. (2007). Ice sheet grounding line dynamics: Steady states, stability, and hysteresis. *Journal of Geophysical Research*, *112*, F03S28. https://doi.org/10.1029/2006JF000664

Schoof, C. (2012). Thermally driven migration of ice-stream shear margins. *Journal of Fluid Mechanics*, *712*, 552–578. https://doi.org/10.1017/jfm.2012.438

Schroeder, D. M., Blankenship, D. D., & Young, D. A. (2013). Evidence for a water system transition beneath Thwaites Glacier, West Antarctica. *Proceedings of the National Academy of Sciences of the United States of America*, *110*(30), 12,225–12,228. https://doi.org/10.1073/pnas.1302828110

Scott, J. B. T., Gudmundsson, G. H., Smith, A. M., Bingham, R. G., Pritchard, H. D., & Vaughan, D. G. (2009). Increased rate of acceleration on Pine Island Glacier strongly coupled to changes in gravitational driving stress. *The Cryosphere*, *3*(1), 125–131. https://doi.org/10.5194/tc-3-125-2009

Sergienko, O. V., & Hindmarsh, R. C. A. (2013). Regular patterns in frictional resistance of ice-stream beds seen by surface data inversion. *Science*, *342*(6162), 1086–1089. https://doi.org/10.1126/science.1243903

Seroussi, H., Morlighem, M., Rignot, E., Mouginot, J., Larour, E., Schodlok, M., & Khazendar, A. (2014). Sensitivity of the dynamics of Pine Island Glacier, West Antarctica, to climate forcing for the next 50 years. *The Cryosphere*, *8*(5), 1699–1710. https://doi.org/10.5194/tc-8-1699-2014

Shapiro, N. M., & Ritzwoller, M. H. (2004). Inferring surface heat flux distributions guided by a global seismic model: Particular application to Antarctica. *Earth and Planetary Science Letters*, *223*(1–2), 213–224. https://doi.org/10.1016/j.epsl.2004.04.011

Shen, Q., Wang, H., Shum, C. K., Jiang, L., Hsu, H. T., & Dong, J. (2018). Recent high-resolution Antarctic ice velocity maps reveal increased mass loss in Wilkes Land, East Antarctica. *Scientific Reports*, *8*(1), 4477. https://doi.org/10.1038/s41598-018-22765-0

Shepherd, A., Wingham, D., & Rignot, E. (2004). Warm ocean is eroding West Antarctic Ice Sheet. *Geophysical Research Letters*, *31*, L23402. https://doi.org/10.1029/2004GL021106

Smith, A. M., Jordan, T. A., Ferraccioli, F., & Bingham, R. G. (2013). Influence of subglacial conditions on ice stream dynamics: Seismic and potential field data from Pine Island Glacier, West Antarctica. *Journal of Geophysical Research: Solid Earth*, *118*, 1471–1482. https://doi.org/10.1029/2012JB009582

Steig, E. J., Ding, Q., Battisti, D. S., & Jenkins, A. (2012). Tropical forcing of circumpolar deep water inflow and outlet glacier thinning in the Amundsen Sea Embayment, West Antarctica. *Annals of Glaciology*, *53*(60), 19–28. https://doi.org/10.3189/2012AoG60A110

Suckale, J., Platt, J. D., Perol, T., & Rice, J. R. (2014). Deformation-induced melting in the margins of the West Antarctic ice streams. *Journal of Geophysical Research: Earth Surface*, *119*, 1004–1025. https://doi.org/10.1002/2013JF003008

Tulaczyk, S., Kamb, B., Scherer, R. P., & Engelhardt, H. F. (1998). Sedimentary processes at the base of a West Antarctic ice stream: Constraints from textural and compositional properties of subglacial debris. *Journal of Sedimentary Research*, *68*(3), 487–496. https://doi.org/10.2110/jsr.68.487

Tulaczyk, S., Kamb, W. B., & Engelhardt, H. F. (2000a). Basal mechanics of ice stream B, West Antarctica 1. Till mechanics. *Journal of Geophysical Research*, *105*, 463–481. https://doi.org/10.1029/1999JB900329

Tulaczyk, S., Kamb, W. B., & Engelhardt, H. F. (2000b). Basal mechanics of ice stream B, West Antarctica 2. Undrained plastic bed model. *Journal of Geophysical Research*, *105*, 483–494. https://doi.org/10.1029/1999JB900328

van de Berg, W. J., van den Broeke, M. R., Reijmer, C. H., & van Meijgaard, E. (2006). Reassessment of the Antarctic surface mass balance using calibrated output of a regional atmospheric climate model. *Journal of Geophysical Research*, *111*, D11104. https://doi.org/10.1029/2005JD006495

van der Wel, N., Christoffersen, P., & Bougamont, M. (2013). The influence of subglacial hydrology on the flow of Kamb Ice Stream, West Antarctica. *Journal of Geophysical Research: Earth Surface*, *118*, 97–110. https://doi.org/10.1029/2012JF002570

Vaughan, D. G., Corr, H. F. J., Ferraccioli, F., Frearson, N., O'Hare, A., Mach, D., et al. (2006). New boundary conditions for the West Antarctic ice sheet: Subglacial topography beneath Pine Island Glacier. *Geophysical Research Letters*, *33*, L09501. https://doi.org/10.1029/2005GL025588

Vieli, A., & Payne, A. J. (2003). Application of control methods for modelling the flow of Pine Island Glacier, West Antarctica. In C. F. Raymond (Ed.). *Annals of Glaciology*, *36*, 197–204.

Vogel, S. W., Tulaczyk, S., Kamb, B., Engelhardt, H., Carsey, F. D., Behar, A. E., et al. (2005). Subglacial conditions during and after stoppage of an Antarctic Ice Stream: Is reactivation imminent? *Geophysical Research Letters*, *32*, L14502. https://doi.org/10.1029/2005GL022563

Walder, J. S., & Fowler, A. (1994). Channelized subglacial drainage over a deformable bed. *Journal of Glaciology*, *40*(134), 3–15. https://doi.org/10.1017/S0022143000003750

Weertman, J. (1972). General theory of water flow at base of a glacier or ice sheet. *Reviews of Geophysics and Space Physics*, *10*(1), 287. https://doi.org/10.1029/RG010i001p00287

Williams, R. S., Ferrigno, J. G., Kent, T. M., & Schoonmaker, W. J. Jr. (1982). Landsat images and mosaics of Antarctica for mapping and glaciological studies. *Annals of Glaciology*, *3*, 321–327.

Winberry, J. P., Anandakrishnan, S., & Alley, R. B. (2009). Seismic observations of transient subglacial water-flow beneath MacAyeal Ice Stream, West Antarctica. *Geophysical Research Letters*, *36*, L11502. https://doi.org/10.1029/2009GL037730

Wingham, D. J., Wallis, D. W., & Shepherd, A. (2009). Spatial and temporal evolution of Pine Island Glacier thinning, 1995-2006. *Geophysical Research Letters*, *36*, L17501. https://doi.org/10.1029/2009GL039126

Wolovick, M. J., Bell, R. E., Creyts, T. T., & Frearson, N. (2013). Identification and control of subglacial water networks under Dome A, Antarctica. *Journal of Geophysical Research: Earth Surface*, *118*, 140–154. https://doi.org/10.1029/2012JF002555

Wright, A. P., Siegert, M. J., Le Brocq, A. M., & Gore, D. B. (2008). High sensitivity of subglacial hydrological pathways in Antarctica to small ice-sheet changes. *Geophysical Research Letters*, *35*, L17504. https://doi.org/10.1029/2008GL034937